

## Article

# The Effect of Nb<sub>2</sub>O<sub>5</sub> Precursor on KNN-Based Ceramics' Piezoelectricity and Strain Temperature Stability

Ruilin Han, Tingting Gao, Yining Xie, Lixu Xie, Yuan Cheng, Xu Li , Hao Chen, Jie Xing \* and Jianguo Zhu \*

College of Materials Science and Engineering, Sichuan University, Chengdu 610064, China

\* Correspondence: xingjie@scu.edu.cn (J.X.); nic0400@scu.edu.cn (J.Z.)

**Abstract:** The performance of potassium sodium niobate ((K, Na) NbO<sub>3</sub>, KNN)-based lead-free piezoelectric ceramics has significantly improved over the past decade. However, the performance bottlenecks of KNN-based ceramics cannot be ignored. Here, the Nb<sub>2</sub>O<sub>5</sub> precursor is obtained after thermal pretreatment, which can evidently improve the piezoelectric properties and strain temperature stability of KNN-based ceramics. With the help of the Nb<sub>2</sub>O<sub>5</sub> precursor treated at 800 °C, the optimal piezoelectric constant  $d_{33}$  of 303 pC/N, inverse piezoelectric constant  $d_{33}^*$  of 378 pm/V, Curie temperature  $T_C$  of 310 °C and electromechanical coupling factor  $k_p$  of 42% are obtained, and the value of  $d_{33}$  improves by about 30% compared with that of the ceramic prepared with untreated Nb<sub>2</sub>O<sub>5</sub> as raw material. Additionally, in comparison with the strain temperature stability of the ceramics prepared with untreated Nb<sub>2</sub>O<sub>5</sub> as raw material, the temperature stability is enhanced. Therefore, this study provides a useful approach to break the existing performance bottleneck and further improve the properties of KNN-based ceramics.



**Citation:** Han, R.; Gao, T.; Xie, Y.; Xie, L.; Cheng, Y.; Li, X.; Chen, H.; Xing, J.; Zhu, J. The Effect of Nb<sub>2</sub>O<sub>5</sub> Precursor on KNN-Based Ceramics' Piezoelectricity and Strain Temperature Stability. *Crystals* **2022**, *12*, 1778. <https://doi.org/10.3390/cryst12121778>

Academic Editors: Maria Gazda, Michele Iafisco, Dawei Wang and Shujun Zhang

Received: 31 October 2022

Accepted: 3 December 2022

Published: 7 December 2022

**Publisher's Note:** MDPI stays neutral with regard to jurisdictional claims in published maps and institutional affiliations.



**Copyright:** © 2022 by the authors. Licensee MDPI, Basel, Switzerland. This article is an open access article distributed under the terms and conditions of the Creative Commons Attribution (CC BY) license (<https://creativecommons.org/licenses/by/4.0/>).

**Keywords:** potassium sodium niobate; Nb<sub>2</sub>O<sub>5</sub> precursor; piezoelectric properties; temperature stability

## 1. Introduction

Since Jaffe discovered the piezoelectric properties of PZT [1], lead-based ceramics have dominated the piezoelectric ceramics market. However, Pb-based ceramics has caused a number of environmental problems, due to the toxicity of lead. Because of concerns about environmental protection, a series of laws, such as the Restriction of Hazardous Substances Directive (RoHS), have been issued to limit the production and applications of lead-based ceramics [2,3]. Due to their excellent piezoelectric properties, potassium sodium niobate KNN-based ceramics are considered as one of the most promising choices to replace lead-based ceramics [4,5].

In the current research, the modification routes of KNN through doping are used to shift the phase transformation temperatures and build phase boundaries near room temperature [6–9]. Past research on KNN-based ceramics has always focused on the influence of external element doping on their properties, but ignored the influence of raw materials. The properties of ceramics strongly depend on the raw materials, not only because of the unknown trace elements in the raw materials, but also because of the variety of crystal structures of uncertain proportions in raw materials. As the raw material with the largest amount of KNN-based ceramics, any change in phase composition of Nb<sub>2</sub>O<sub>5</sub> may affect the properties of ceramics. Previous studies have reported that there are monoclinic and orthorhombic crystal structures in Nb<sub>2</sub>O<sub>5</sub> [10], and the Nb<sub>2</sub>O<sub>5</sub> that we use in the preparation of KNN-based ceramics is orthorhombic [11–15]. However, our recent experiments find that a small amount of Nb<sub>2</sub>O<sub>5</sub> with a monoclinic structure, instead of Nb<sub>2</sub>O<sub>5</sub> with orthorhombic structure, will significantly improve the piezoelectric properties and strain temperature stability of KNN-based ceramics.

For KNN-based ceramics, the most commonly used perovskite additive (Bi<sub>0.5</sub>Na<sub>0.5</sub>)ZrO<sub>3</sub> can effectively shift the transition temperatures of rhombohedral–orthorhombic ( $T_{R-O}$ ) and

orthorhombic–tetragonal ( $T_{O-T}$ ) phases simultaneously, finally constructing phase boundaries such as R-O-T or R-T around room temperature [16–21]. In addition,  $\text{Fe}_2\text{O}_3$  can also be used to modulate the phase boundaries and improve the densification, microstructure, piezoelectric, as well as ferroelectric, properties of KNN ceramics [22,23]. Hence, the introduction of BNZ and  $\text{Fe}_2\text{O}_3$  can effectively increase the electric properties of KNN-based ceramics. In this paper, a  $0.95(\text{K}_{0.45}\text{Na}_{0.55})\text{NbO}_3\text{-}0.05(\text{Bi}_{0.5}\text{Na}_{0.5})\text{ZrO}_3\text{-}0.4\%\text{Fe}_2\text{O}_3$  (KNN-BNZ-Fe) system is designed, and pretreated  $\text{Nb}_2\text{O}_5$  in different pretreated temperatures is used, following its conversion from an orthorhombic structure to a monoclinic structure, to verify the above findings systematically. Under the reactions of  $\text{Nb}_2\text{O}_5$  with an orthorhombic structure and monoclinic structure, the piezoelectric properties of the ceramics change; the  $d_{33}$  value of the ceramics increases from 231 pC/N to 303 pC/N with a 31% increase and the  $d_{33}^*$  values of the ceramics rise from 319 pm/V to 378 pm/V with a 16% increase. Furthermore, the temperature stability of the ceramics significantly improves. KNN-based ceramics with higher piezoelectric properties and better temperature stability are prepared on the basis of this work. In addition, the related physical mechanisms are also explained.

## 2. Materials and Methods

The  $0.95(\text{K}_{0.45}\text{Na}_{0.55})\text{NbO}_3\text{-}0.05(\text{Bi}_{0.5}\text{Na}_{0.5})\text{ZrO}_3\text{-}0.4\%\text{Fe}_2\text{O}_3$  (KNN-BNZ-Fe) ceramics are fabricated through solid-phase synthesis.  $\text{K}_2\text{CO}_3$  (99.0%),  $\text{Na}_2\text{CO}_3$  (99.8%),  $\text{ZrO}_2$  (99.0%),  $\text{Bi}_2\text{O}_3$  (99.999%),  $\text{Fe}_2\text{O}_3$  (99.99%) and  $\text{Nb}_2\text{O}_5$  (99.5%) are used as raw materials.  $\text{Nb}_2\text{O}_5$  is heated under 600 °C, 700 °C, 800 °C, 850 °C, 900 °C, 950 °C and 1000 °C, respectively, in a sintering furnace for 2 h to produce ceramics with different proportions of orthorhombic structure and monoclinic structure compositions. In order to more easily distinguish between the KNN-BNZ-Fe ceramics prepared with  $\text{Nb}_2\text{O}_5$  as the raw material at different pretreated temperatures, the KNN-BNZ-Fe ceramics prepared by untreated  $\text{Nb}_2\text{O}_5$  are labeled as KNN-UN, and the other KNN-BNZ-Fe ceramics prepared by the  $\text{Nb}_2\text{O}_5$  precursor pretreated at 600 °C, 700 °C, 800 °C, 850 °C, 900 °C, 950 °C and 1000 °C are labeled as KNN-600, KNN-700, KNN-800, KNN-850, KNN-900, KNN-950 and KNN-1000, respectively. Other detailed experimental processes can be observed in previous reports by our group [24] with the patent CN. 2022113031604.

After aging for 24 h, the piezoelectric constant ( $d_{33}$ ) values of the poled samples are measured using a quasi-static  $d_{33}$  testing meter (ZJ-3A, Institute of Acoustics, Chinese Academy of Sciences, China), while an impedance analyzer (HP 4294A, Agilent, Santa Clara, USA) is used to obtain the planar electromechanical coupling factor ( $k_p$ ) values and mechanical quality factor ( $Q_m$ ) values. For the crystal structures of the ceramics, the X-ray diffraction (XRD) patterns of grinded powder of the ceramics is measured using an X' Pert Pro MPD (DY120 PANalytical, Almelo, Netherlands) with Cu radiation ( $\lambda\text{K}\alpha_1 = 1.54056\text{\AA}$ ), operating at 40 kV and 30 mA, a step scan of  $0.02^\circ/\text{step}$  and a counting time of 30 s per step. The dielectric constants ( $\epsilon_r$ ) against the temperature curves are collected by an LCR analyzer (HP 4980, Agilent, Santa Clara, USA). The surface morphologies of the sintered pellet are characterized using a scanning electron microscope (SEM, Se3400N, Hitachi, Tokyo, Japan). The domain structures are investigated using a piezo-response force microscope (PFM, Asylum Research, Oxford, UK). The field-dependent polarization  $P$ - $E$  loops, unipolar and bipolar  $S$ - $E$  curves are measured using a ferroelectric analyzer (TF Analyzer 2000, aix ACCT, Aachen, Germany).

## 3. Results and Discussion

Figure 1 shows the XRD patterns of the pretreated  $\text{Nb}_2\text{O}_5$  powder samples at different temperatures. The un-pretreated  $\text{Nb}_2\text{O}_5$  displays a typical orthorhombic structure [9], and when the pretreatment temperature rises to 800 °C, new peaks appear, indicating the appearance of monoclinic  $\text{Nb}_2\text{O}_5$  [15] and the coexistence of orthorhombic and monoclinic structures. As the temperature continues to increase from 850 °C to 1000 °C, only the monoclinic  $\text{Nb}_2\text{O}_5$  remains.

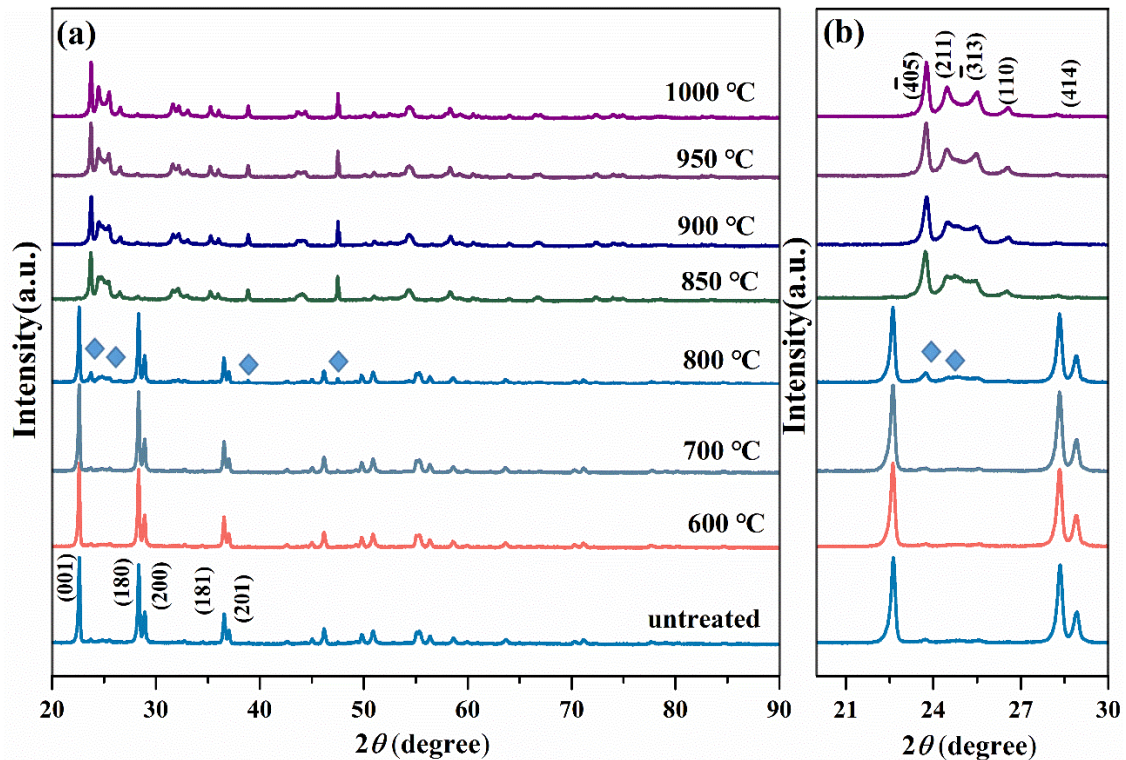


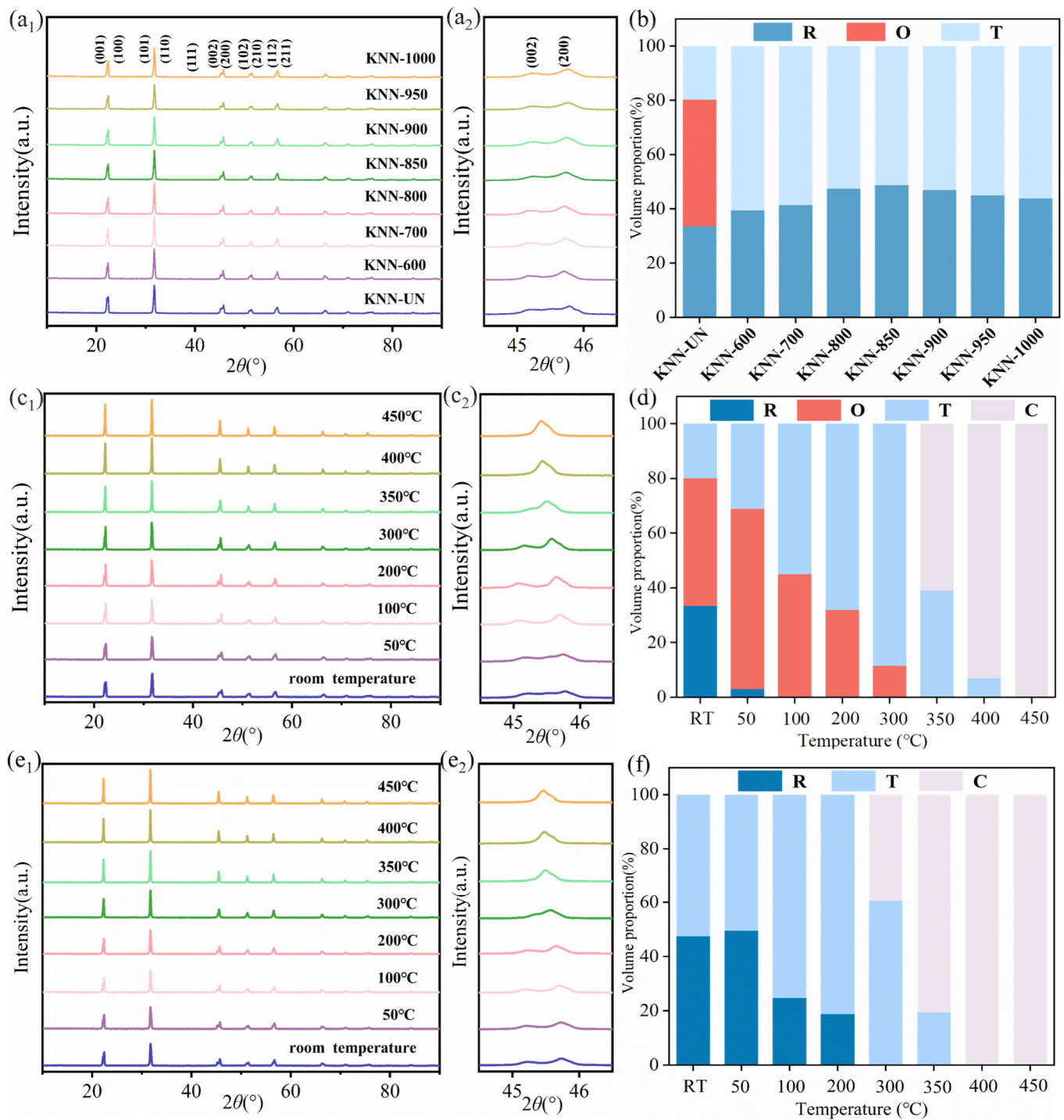
**Figure 1.** XRD patterns of  $\text{Nb}_2\text{O}_5$  precursor powders treated at different temperatures, in the following ranges: (a)  $20^\circ < \theta < 90^\circ$ ; (b)  $20^\circ < \theta < 30^\circ$ . The blue square indicates the presence of monoclinic  $\text{Nb}_2\text{O}_5$ .

We compared the pure  $\text{K}_{0.45}\text{Na}_{0.45}\text{NbO}_3$  (KNN) and  $\text{K}_{0.45}\text{Na}_{0.45}\text{NbO}_3\text{-}0.4\%\text{Fe}_2\text{O}_3$  (KNN-Fe), which presented pure perovskite orthorhombic structures, with  $0.95(\text{K}_{0.45}\text{Na}_{0.55})\text{NbO}_3\text{-}0.05(\text{Bi}_{0.5}\text{Na}_{0.5})\text{ZrO}_3$  (KNN-BNZ), which presented three-phase coexistence states of R, O and T phases. KNN-UN (KNN-BNZ-Fe) ceramics also displays evidence of rhombohedral–orthorhombic–tetragonal (R-O-T) multiphase coexistence at room temperature, as shown in Figure S1. The Rietveld refinement for KNN, KNN-Fe, KNN-BNZ and KNN-UN is carried out to confirm the crystal structures, which are refined by the  $R3m$  (rhombohedral),  $Amm2$  (orthorhombic) and  $P4mm$  (tetragonal) symmetry models, as shown in Figure S2, confirming the O phase of KNN and KNN-Fe and R-O-T multiphase coexistence in KNN-BNZ and KNN-BNZ-Fe ceramics. The corresponding parameters obtained from the Rietveld refinement are shown in Table S1. Figure 2(a1,a2) show the XRD patterns of all the studied KNN-BNZ-Fe ceramics with different  $\text{Nb}_2\text{O}_5$  precursors. All the diffraction peaks in this scanning region suggest a perovskite structure. The Rietveld refinement for KNN-UN is carried out to confirm the existence of KNN-UN ceramics with rhombohedral–orthorhombic–tetragonal (R-O-T) multiphase coexistence at room temperature, which is refined by the  $R3m$  (rhombohedral),  $Amm2$  (orthorhombic) and  $P4mm$  (tetragonal) symmetry models, and the Rietveld refinement for KNN-600~1000 is carried out to confirm the coexistence of rhombohedral–tetragonal (R-T) multiphases, which are refined using the  $R3m$  (rhombohedral) and  $P4mm$  (tetragonal) symmetry models [16], as shown in Figure S3. The corresponding refined parameters are listed in Table S2 in the supporting information. Good fitting results between the original data and calculated lines can be observed, indicating the accuracy of the refinements. The specific phase contents based on the Rietveld refinement of XRD patterns of each sample are shown in Figure 2b. The R-O-T phases coexist in KNN-UN, and R-T phases coexist in KNN-600~1000, correspondingly. The change in the content of the R phase shows a trend of first increasing and then decreasing, reaching the maximum value at KNN-800, which is the opposite of the T phase. The changes in the XRD patterns of KNN-UN with the increase in temperature from

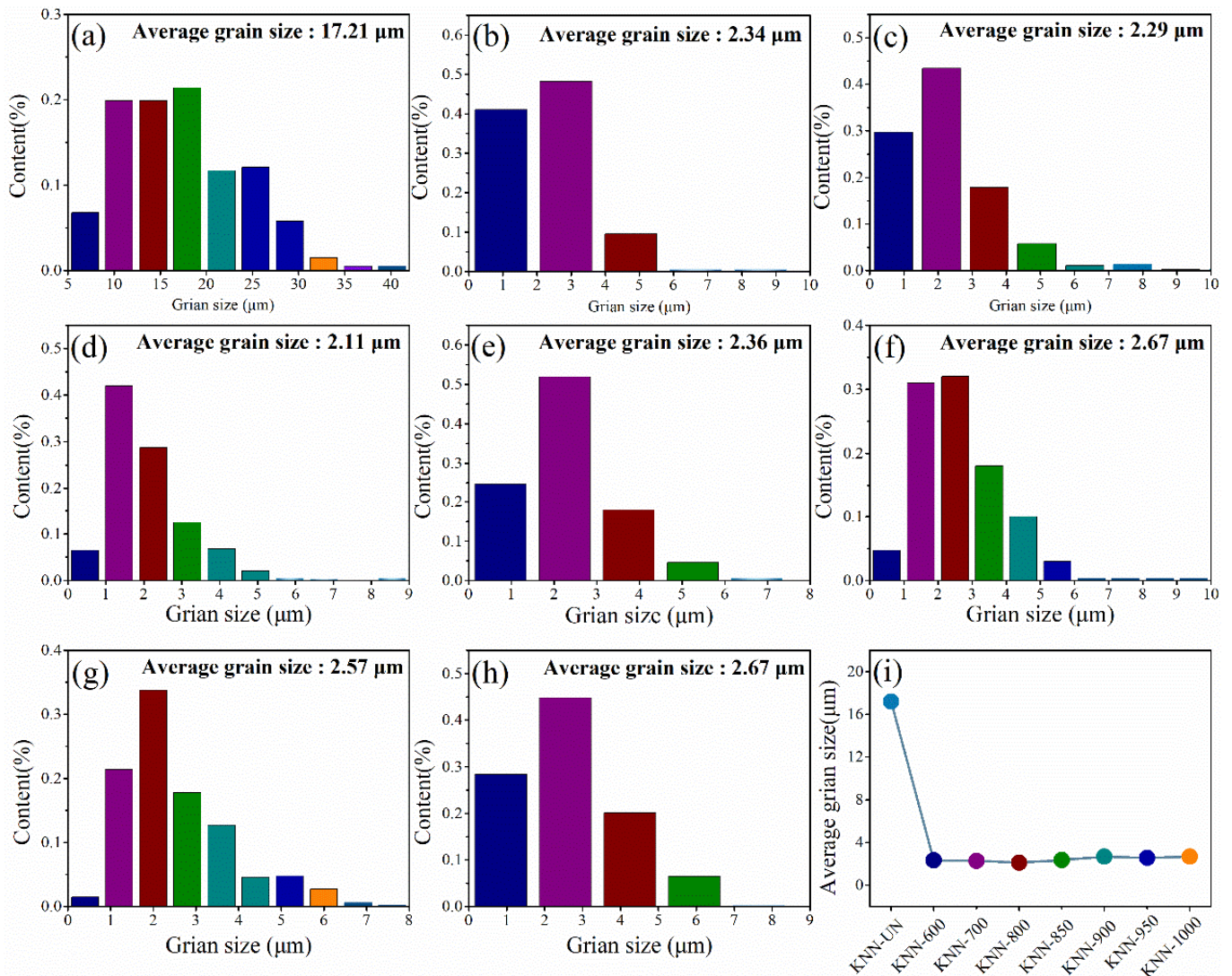
room temperature to 450 °C are measured as shown in Figure 2(c1,c2). Rietveld plots of the KNN-UN ceramic are displayed in Figure S4. The specific phase structure proportion is reflected in Figure 2d and the corresponding refined parameters obtained through Rietveld refinement are listed in Table S3, which are in good agreement with the changes in XRD diffraction peaks of the KNN-UN ceramic. The composition and content of the ceramic phases change dramatically in this temperature range. The R phase of KNN-UN decreases rapidly as the temperature rises from room temperature to 100 °C. When the temperature rises to 200 °C, the ceramic maintains the composition of the O and T phases. When the temperature reaches 300 °C, the peaks of (002) and (200) begin to merge, meaning the appearance of the cubic (C) phase. The peaks of (002) and (200) completely merge into one peak until 400 °C, revealing that the ceramics have completely changed into the C phase. The temperature dependence of the XRD patterns for KNN-800 is measured as shown in Figure 2(e1,e2). Rietveld plots of the KNN-800 ceramic are displayed in Figure S5. The specific phase structure proportion from room temperature to 450 °C is reflected in Figure 2f and the corresponding refined parameters are listed in Table S4 in the supporting information. From room temperature to 100 °C, the content of the R phase gradually decreases until it disappears, accompanied by the increase in the T phase content. With further increasing temperature (200 °C < T < 300 °C), two splitting peaks shift close to each other, the T phase dominates and the emergence of the C phase in this temperature range and temperature-induced lattice distortion can be observed [25]. When the temperature reaches 350 °C and above, the peak completely merges into a single peak, showing that the ceramic has mostly transformed into the C phase.

Normally, the piezoelectric properties of KNN-based ceramics are closely related to their microstructures. Therefore, the SEM micrographs for KNN-UN~1000 are shown in Figure S6. The KNN-UN ceramic is evidently different from other ceramics, as all the sizes of the grains of KNN-UN are on a micron and uniform scale, with fine pores distributed between the grains. The uniformly distributed pores of the KNN-UN ceramic may be caused by the incomplete coupling between large grains. However, in the coupling effect of small grains, the holes of KNN-800 ceramics are obviously reduced, and the holes in other ceramics may be caused by the emergence of oxygen vacancies, resulting in the volatilization of alkali metals [26]. Further elaboration of the grains is due to the different reaction rates of K/Na and Nb<sub>2</sub>O<sub>5</sub> with different crystal structures, resulting in irregular growth behavior [27]. Figure 3a–h show the grain size statistics of KNN-UN~1000, and the average grain size distributions of all the ceramics are shown in Figure 3i, displaying a trend of initial decline and rise afterwards, which is the least noticeable for the KNN-800 ceramic.

Generally, the dielectric constant versus temperature ( $\epsilon_r - T$ ) curves can also identify the phase structure related to the compositions. Therefore, the changes in the permittivity of different ceramics with temperatures between –120 °C and 200 °C have been measured, as shown in Figure S7a–h. As we can observe, there are two peaks in the  $\epsilon_r - T$  diagram of the KNN-UN ceramic, which indicates two phase transitions below 200 °C, but only a single peak in those of KNN-600~1000, which indicates one single phase transition below 200 °C. With the increase in the pretreatment temperature of Nb<sub>2</sub>O<sub>5</sub>, the  $T_{R-T}$  values of the ceramics first increase, which is then followed by a decline, consistent with the changing trend of the R phase content in Figure 2b. In order to further characterize the phase transition of the ceramics within a high temperature range, the  $\epsilon_r - T$  curves of the sample from room temperature to 450 °C are measured as shown in Figure S7i. It can be observed that the  $T_C$  values of the KNN-UN to KNN-800 ceramics decrease from 347 °C to 310 °C gradually, and increase to 334 °C for KNN-850, then remaining almost unchanged. According to the analysis of the previous experimental results [9], KNN-UN to KNN-700 ceramics are prepared using Nb<sub>2</sub>O<sub>5</sub> with an orthonormal phase, while KNN-850 to KNN-1000 ceramics are made from Nb<sub>2</sub>O<sub>5</sub> with a monoclinic phase, indicating that the  $T_C$  of the ceramics prepared with orthonormal-phase Nb<sub>2</sub>O<sub>5</sub> as raw material will decrease slightly.



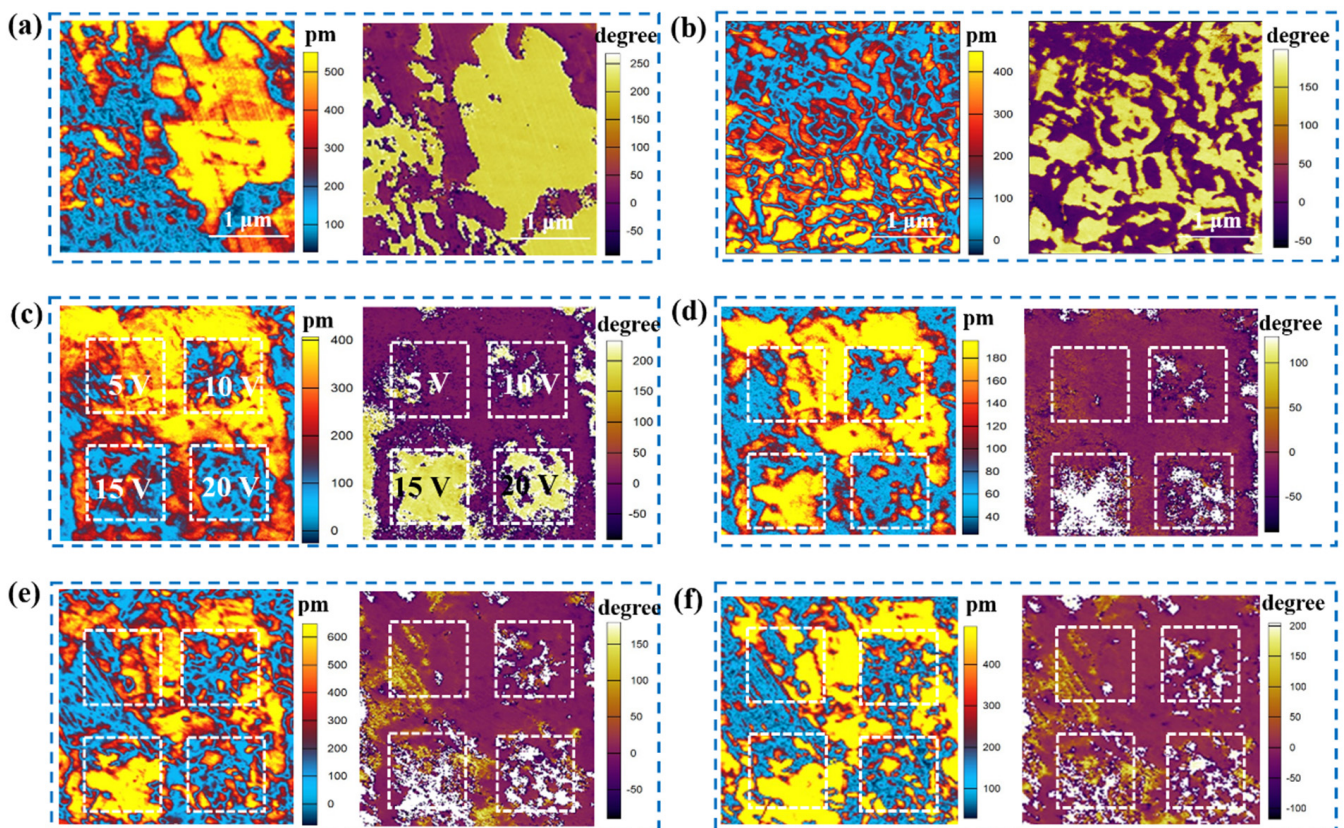
**Figure 2.** (a1) XRD pattern of KNN-BNZ-Fe ceramics, in the following range:  $10^\circ < \theta < 90^\circ$ ; (a2)  $44^\circ < \theta < 47^\circ$ . (b) The phase content of KNN-BNZ-Fe ceramics with different  $\text{Nb}_2\text{O}_5$  precursors; (c1) XRD patterns of KNN-UN measured from room temperature to  $450^\circ\text{C}$ , in the following range:  $10^\circ < \theta < 90^\circ$ ; (c2)  $44^\circ < \theta < 47^\circ$ . (d) The change in phase content of KNN-UN from room temperature to  $450^\circ\text{C}$ ; (e1) XRD patterns of KNN-800 measured from room temperature to  $450^\circ\text{C}$ , in the following range:  $10^\circ < \theta < 90^\circ$ ; (e2)  $44^\circ < \theta < 47^\circ$ ; (f) The change in phase content of KNN-800 from room temperature to  $450^\circ\text{C}$ .



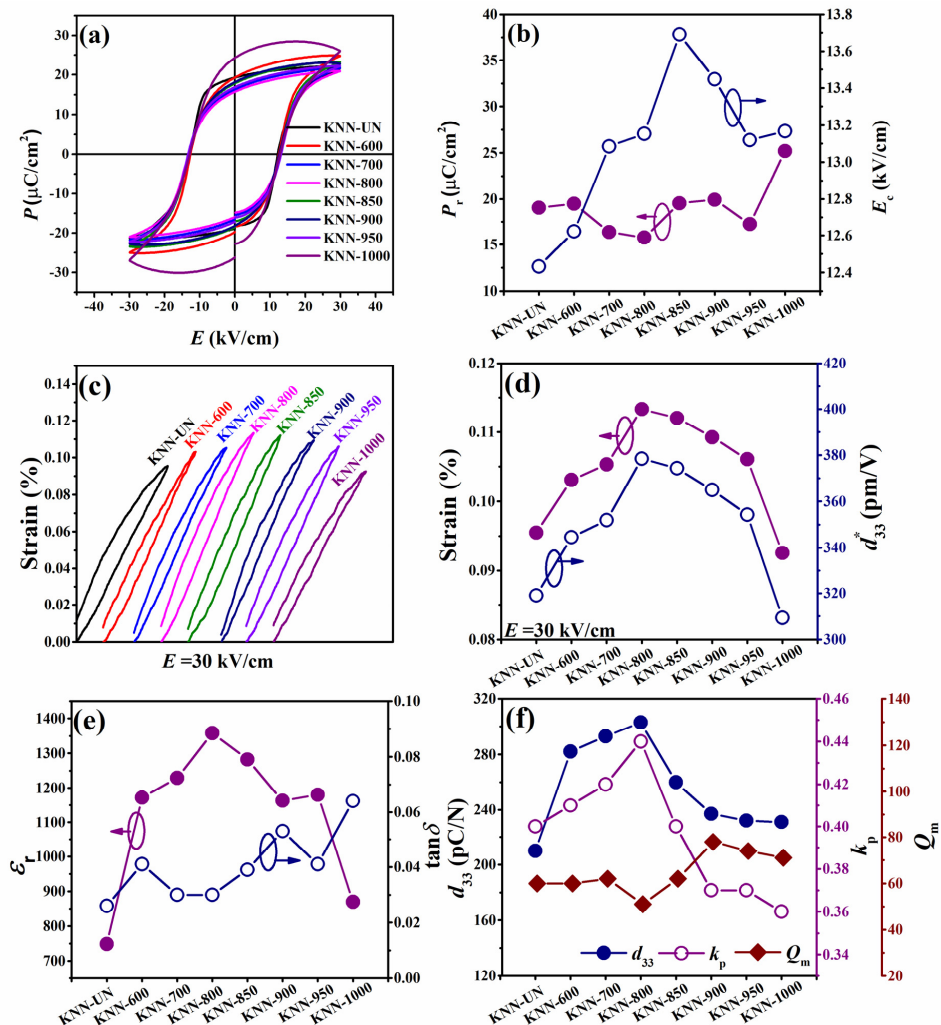
**Figure 3.** Grain size statistics: (a) KNN-UN; (b) KNN-600; (c) KNN-700; (d) KNN-800; (e) KNN-850; (f) KNN-900; (g) KNN-950; (h) KNN-1000; (i) average grain size distribution of KNN-UN~KNN-1000 ceramics.

As the electrical properties of perovskite piezoelectric ceramics are closely related to their domain structures [28–31], and to further analyze the contributions of domain structures to the temperature stability of the piezoelectric effect, the piezo-response force microscopy (PFM) amplitude and phase images are investigated. The PFM images for KNN, KNN-Fe and KNN-BNZ ceramics are presented in Figure S8. Large, blocky and strip domains exist in both KNN and KNN-Fe ceramics. With the addition of BNZ, the domain of KNN-BNZ becomes smaller and more uniform. The KNN-UN and KNN-800 ceramics are measured as shown in Figure 4a,b. The domain boundaries can be observed from the amplitude images because the domain boundaries display almost no piezoelectric response, and the phase images correspond well to their amplitude images [32]. However, there is a considerable gap between the amplitude image of KNN-UN and that of KNN-800, that is, unevenly distributed micron and submicron domains exist in the amplitude image of the KNN-UN ceramic, and evenly distributed submicron domains exist in the amplitude image of the KNN-800 ceramic. Larger domains cannot be easily inverted under applied electric fields, which may be result in low piezoelectric performances. The Litho mode of PFM is used to check the domain-switching dynamic behavior. Firstly, the four small areas of  $1 \times 1 \mu\text{m}^2$  on the KNN-800 ceramic are subjected to different bias voltages (5 V,

10 V, 15 V and 20 V, respectively). The PFM mappings are recorded after removing the bias voltage. As presented in the Figure 4c, a bias voltage equal to or greater than 15 V can reverse the ferroelectric domains of ceramics and cause them to approach saturation. The in situ PFM images from room temperature to 100 °C are analyzed to further check the thermal stability of the switched domain under different temperatures. The Litho mode of the domains, including the amplitude and phase images of the KNN-800 ceramic at 20 °C, 60 °C, 80 °C and 100 °C, are shown in Figure 4c,e. As the temperature increases from 20 °C to 60 °C, the amplitude and phase response domain decreases slightly, due to the change in domain orientation caused by thermal excitation. All the domains will align with the electric field direction in the initial state of the Litho mode. With increasing temperatures, thermal excitation will disrupt the domain orientation, finally decreasing the amplitude of the domains [32]. As the applied electric field decreases, the thermal excitation phenomenon becomes more obvious. When temperature increases to 80 °C, the response domain decreases sequentially, but the amplitude increases suddenly, which may be caused by the phase transition close to  $T_{R-T}$ . The synergistic effect of the reduction in the response domain and the increase in the amplitude may be the reason for the good temperature stability of its external performance at this temperature. Finally, the amplitude response domain and intensity of KNN-800 decreases slightly at 100 °C, indicating good temperature stability.



**Figure 4.** (a) The piezo-response force microscopy (PFM) amplitude and phase images of KNN-UN with a scan area of  $3 \mu\text{m} \times 3 \mu\text{m}$ ; (b) the piezo-response force microscopy (PFM) amplitude and phase images of KNN-800 with a scan area of  $3 \mu\text{m} \times 3 \mu\text{m}$ ; (c–f) the Litho mode of KNN-800 at 20 °C, 60 °C, 80 °C and 100 °C, including amplitude and phase images with a scan area of  $3 \mu\text{m} \times 3 \mu\text{m}$ .



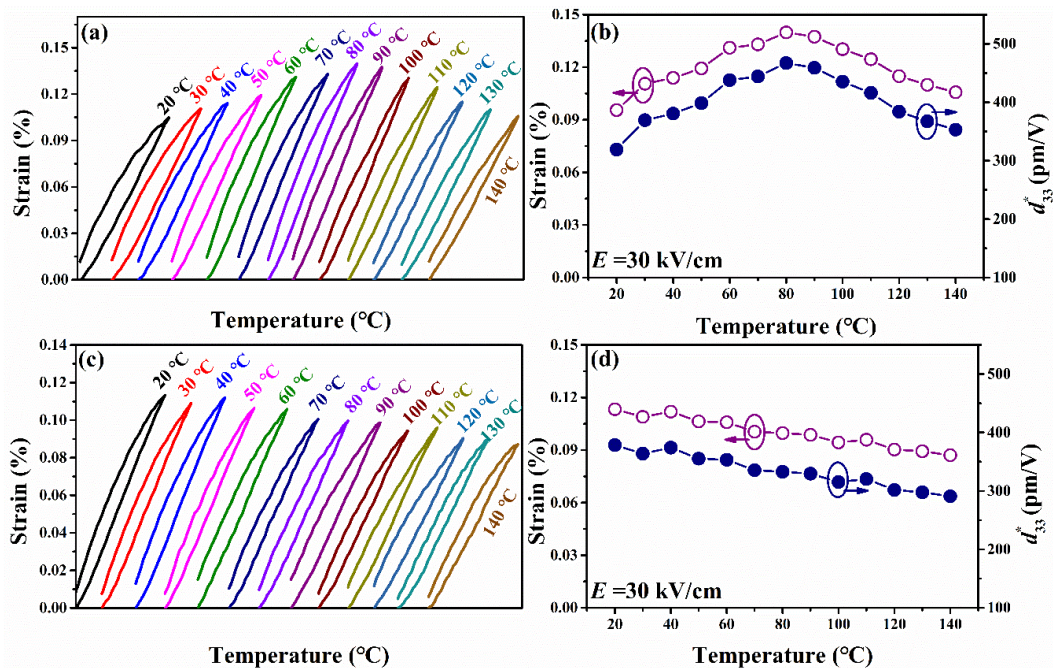
**Figure 5.** (a) The  $P - E$  loops; (b) the  $P_r$  and  $E_c$  values; (c) unipolar strain curves; (d) strain and  $d_{33}$  values; (e)  $\epsilon_r$  and  $\tan\delta$  values; (f)  $d_{33}$ ,  $k_p$  and  $Q_m$  values.

Figure 5a shows the  $P - E$  hysteresis loops of KNN-UN~1000, as all the ceramics present typical ferroelectric loops. The  $P_r$  (remnant polarization) and  $E_c$  (coercive electric field) are shown in Figure 5b. The  $P_r$  values of the ceramics first decrease then increase, and the minimum value is recorded for the KNN-800 ceramic. The decrease in  $P_r$  is mainly due to the reduced grain size because of the domain wall clamping from grain boundaries [33]. In addition, the  $T_{R-T}$  values of KNN-600~950 ceramics near room temperature can cause the instability of the polarization state and the polarization direction can be easily rotated by external fields, which results in enhanced  $P_r$  values. In perovskite ceramics, the phase structure at low temperatures often presents higher spontaneous polarization values [34], so the high content of the R phase in KNN ceramics results in higher  $P_r$  values. Hence, the KNN-based ceramics with the pretreated  $\text{Nb}_2\text{O}_5$  powder at different temperatures can decrease the  $P_r$  values and also increase them. However, the abnormal increase for KNN-1000 is mainly due to the leakage current of the ceramic, meaning that the measured value is an exchange charge rather than a real  $P_r$  [35]. With the increase in  $\text{Nb}_2\text{O}_5$  pretreatment temperatures, the  $E_c$  values show an upward trend first, and then decrease. From the point of view of crystallographic physics, the domain wall motion in a tetragonal structure is more easily performed than the domain wall motion of a rhombohedral structure. Hence, a rhombohedral structure requires a higher  $E_c$  in the 180 domain and the  $E_c$  in a tetragonal structure is smaller than that of a rhombohedral structure. According to the XRD patterns and Rietveld refinement, the change in the content

of the R phase shows a trend of first increasing and then decreasing, and the maximum value is reported for KNN-800, which is the opposite of the T phase. In addition, the piezoelectric properties of ferroelectric polycrystals are closely associated with domain morphologies [31], and the decreasing grain sizes can enhance domain wall mobility and increase the orientation resistance of the domains, eventually leading to an increased coercive field [36]. The unipolar curves of KNN-UN~1000 ceramics are shown in Figure 5c.

The strain values and  $d_{33}^*$  ( $d_{33}^* = S_{max}/E_{max}$ ) values (shown in Figure 5d) firstly increase and reach their maximum values for the KNN-850 ceramic; with further increasing  $Nb_2O_5$  pretreatment temperatures, the strain values and  $d_{33}^*$  values begin to fall. The  $d_{33}^*$  reaches its maximum value ( $\sim 378$  pm/V) for KNN-800; the coexistence phase boundary of multiple ferroelectric phases can result in the highest values of  $S_{uni}$  and  $d_{33}^*$  for KNN-800. The changes in the dielectric constant ( $\epsilon_r$ ) and dielectric loss ( $\tan \delta$ ) are shown in Figure 5e. The  $\epsilon_r$  values first decrease then increase and the  $\tan \delta$  values remain almost unchanged with different  $Nb_2O_5$  pretreatment temperatures. The piezoelectric constant  $d_{33}$  values and electromechanical coupling factor ( $k_p$ ), as shown in Figure 5f, first increase then decrease, reaching their maximum values for KNN-800. The quality factor ( $Q_m$ ) values are also shown in Figure 5f, showing the trend of first decreasing and then increasing. The optimal  $d_{33}^*$  values of 303 pC/N and  $d_{33}^*$  of 378 pm/V, with a  $k_p$  value of 42%, are obtained for KNN-800.

Temperature stability is an indispensable and non-negligible area of research. The temperature dependence of unipolar strain curves, strain values and  $d_{33}^*$  values of KNN-UN and KNN-800 are shown in Figure 6a–d. It can be observed that the temperature stability behaviors of KNN-UN and KNN-800 ceramics show significant differences. Both the strain and  $d_{33}^*$  values of KNN-UN ceramics show an increasing trend first, then decrease with increasing temperatures. The variations in the strain and  $d_{33}^*$  values of KNN-800 ceramics are less noticeable, and demonstrate slow downward trends, showing improved temperature stability.



**Figure 6.** The unipolar S-E curves, strain values and  $d_{33}^*$  values for (a), (c) KNN-UN; (b), (d) KNN-800 ceramics measured under different temperatures.

#### 4. Conclusions

In summary, significant performance improvements of KNN-BNZ-Fe ceramics can be achieved through the pretreatment of the raw material  $\text{Nb}_2\text{O}_5$  from 600 °C to 1000 °C, and its structure and physical origin are revealed. The effect of the pretreatment temperature of  $\text{Nb}_2\text{O}_5$  on the microstructure and electrical properties, as well as strain thermal stability, is illuminated in detail. The change in phase composition and content enhances the piezoelectric properties. The surface morphologies indicate that the pretreatment temperature of  $\text{Nb}_2\text{O}_5$  has a great inhibition effect on grain growth. Correspondingly, both the piezoelectric properties and strain temperature stability of ceramics achieve their optimal value when the raw material  $\text{Nb}_2\text{O}_5$  is pretreated at 800 °C, and an optimal  $d_{33}$  value of 303 pC/N can be obtained for the ceramic, which is improved by about 30% compared with that of the ceramic prepared with untreated  $\text{Nb}_2\text{O}_5$  as raw material. In addition, in comparison with the strain temperature stability of the ceramic prepared with untreated  $\text{Nb}_2\text{O}_5$  as raw material, the temperature stability increases from 30 °C to 150 °C. Therefore, this research reports the enhanced performance of KNN-based ceramics.

**Supplementary Materials:** The following supporting information can be downloaded at <https://www.mdpi.com/article/10.3390/cryst12121778/s1>: Figure S1: XRD patterns of KNN, KNN-Fe, KNN-BNZ, KNN-BNZ-Fe and KNN-UN from (a)  $20^\circ < \theta < 90^\circ$ , (b)  $44^\circ < \theta < 47^\circ$ ; Figure S2: (a–d) The Rietveld refinement for KNN, KNN-Fe, KNN-BNZ, KNN-UN ceramics; Figure S3: (a–h) The Rietveld refinement for KNN-UN, KNN-600, KNN-700, KNN-800, KNN-850, KNN-900, KNN-950, KNN-1000; Figure S4: (a–h) the Rietveld refinement for KNN-UN from room temperature to 450 °C; Figure S5: (a–h) the Rietveld refinement for KNN-800 from room temperature to 450 °C; Figure S6: (a–h) Scanning Electron Microscopy (SEM) micrographs for KNN-UN, KNN-600, KNN-700, KNN-800, KNN-850, KNN-900, KNN-950, KNN-1000; Figure S7: (a–h) The  $\epsilon_r - T$  curves of KNN-UN, KNN-600, KNN-700, KNN-800, KNN-850, KNN-900, KNN-950, KNN-1000 from  $-120^\circ\text{C}$  to  $200^\circ\text{C}$ ; (i) the  $\epsilon_r - T$  curves of KNN-UN, KNN-600, KNN-700, KNN-800, KNN-850, KNN-900, KNN-950, KNN-1000 from room temperature to 450 °C; Figure S8: (a) The piezo-response force microscopy (PFM) amplitude and phase images of KNN with a scan area of  $3\ \mu\text{m} \times 3\ \mu\text{m}$ ; (b) the piezo-response force microscopy (PFM) amplitude and phase images of KNN-Fe with a scan area of  $3\ \mu\text{m} \times 3\ \mu\text{m}$ ; (c) the piezo-response force microscopy (PFM) amplitude and phase images of KNN-BNZ with a scan area of  $3\ \mu\text{m} \times 3\ \mu\text{m}$ ; Table S1: Parameters of KNN, KNN-Fe, KNN-BNZ and KNN-UN ceramics obtained from Rietveld refinement; Table S2: Parameters of KNN-UN~KNN-1000 obtained from Rietveld refinement; Table S3: Parameters of KNN-UN~KNN-1000 obtained from Rietveld refinement; Table S4: Parameters of KNN-UN~KNN-800 obtained from Rietveld refinement.

**Author Contributions:** Conceptualization, J.X., R.H. and T.G.; Formal analysis, R.H., L.X. and Y.C.; Software, X.L.; Data curation, R.H. and H.C.; Writing—original draft, R.H., T.G. and Y.X.; Writing—review and editing, J.X. and J.Z. All authors have read and agreed to the published version of the manuscript.

**Funding:** The Key-Area Research and Development Program of Guangdong Province of China (2020B0109380001), the National Natural Science Foundation of China (12004267, 52032007), the Fundamental Research Funds for the Central Universities of China and the Natural Science Foundation of Sichuan Province (2022NSFSC0376).

**Institutional Review Board Statement:** Not applicable.

**Informed Consent Statement:** Not applicable.

**Data Availability Statement:** Not applicable.

**Acknowledgments:** This work is supported by the Key-Area Research and Development Program of Guangdong Province of China (2020B0109380001), the National Natural Science Foundation of China (12004267, 52032007), the Fundamental Research Funds for the Central Universities of China and the Natural Science Foundation of Sichuan Province (2022NSFSC0376).

**Conflicts of Interest:** The authors declare no conflict of interest.

## References

1. Jaffe, B.; Cook, W.R.; Jaffe, H. *Piezoelectric Ceramics*; Academic Press: New York, NY, USA, 1971.
2. Shrout, T.R.; Zhang, S.J. Lead-free piezoelectric ceramics: Alternatives for PZT? *J. Electroceram.* **2007**, *19*, 113–126. [[CrossRef](#)]
3. Zhao, C.; Huang, Y.; Wu, J. Multifunctional barium titanate ceramics via chemical modification tuning phase structure. *Info. Mat.* **2020**, *2*, 1163–1190. [[CrossRef](#)]
4. Zhou, C.; Zhang, J.; Yao, W.; Liu, D.; He, G. Remarkably strong piezoelectricity, rhombohedral-orthorhombic-tetragonal phase coexistence and domain structure of (K,Na)(Nb,Sb)O<sub>3</sub>-(Bi,Na)ZrO<sub>3</sub>-BaZrO<sub>3</sub> ceramics. *J. Alloy Compd.* **2020**, *820*, 153411. [[CrossRef](#)]
5. Tao, H.; Wu, H.; Liu, Y.; Zhang, Y.; Wu, J.; Li, F.; Lyu, X.; Zhao, C.; Xiao, D.; Zhu, J.; et al. Ultrahigh Performance in Lead-Free Piezoceramics Utilizing a Relaxor Slush Polar State with Multiphase Coexistence. *J. Am. Chem. Soc.* **2019**, *141*, 13987–13994. [[CrossRef](#)]
6. Zhang, M.H.; Wang, K.; Du, Y.J.; Dai, G.; Sun, W.; Li, G.; Hu, D.; Thong, H.C.; Zhao, C.; Xi, X.Q.; et al. High and Temperature-Insensitive Piezoelectric Strain in Alkali Niobate Lead-free Perovskite. *J. Am. Chem. Soc.* **2017**, *139*, 3889–3895. [[CrossRef](#)]
7. Cen, Z.; Yu, Y.; Zhao, P.; Chen, L.; Zhu, C.; Li, L.; Wang, X. Grain configuration effect on the phase transition, piezoelectric strain and temperature stability of KNN-based ceramics. *J. Mater. Chem. C* **2019**, *7*, 1379–1387. [[CrossRef](#)]
8. Liu, Q.; Zhang, Y.; Gao, J.; Zhou, Z.; Wang, H.; Wang, K.; Zhang, X.; Li, L.; Li, J.-F. High-performance lead-free piezoelectrics with local structural heterogeneity. *Energy Environ. Sci.* **2018**, *11*, 3531–3539. [[CrossRef](#)]
9. Zhang, J.; Sun, X.; Su, W.; Yao, W.; Zhou, C. Superior piezoelectricity and rhombohedral-orthorhombic-tetragonal phase coexistence of (1-x)(K,Na)(Nb,Sb)O<sub>3</sub>-x(Bi,Na)HfO<sub>3</sub> ceramics. *Scr. Mater.* **2020**, *176*, 108–111. [[CrossRef](#)]
10. Thong, H.-C.; Zhao, C.; Zhu, Z.-X.; Chen, X.; Li, J.-F.; Wang, K. The impact of chemical heterogeneity in lead-free (K, Na)NbO<sub>3</sub> piezoelectric perovskite: Ferroelectric phase coexistence. *Acta Mater.* **2019**, *166*, 551–559. [[CrossRef](#)]
11. Lv, X.; Wu, J.; Zhang, X.X. Tuning the Covalency of A-O Bonds to Improve the Performance of KNN-Based Ceramics with Multiphase Coexistence. *ACS Appl. Mater. Interfaces* **2020**, *12*, 49795–49804. [[CrossRef](#)]
12. Liu, Z.; Zhang, A.; Lu, J.; Xie, B.; Liang, B.; Mao, Y.; Fan, H. Balanced development of dielectric permittivity, loss tangent, and temperature stability in K<sub>0.5</sub>Na<sub>0.5</sub>NbO<sub>3</sub>-based ceramic capacitors. *J. Alloy Compd.* **2020**, *817*, 152798. [[CrossRef](#)]
13. Chen, K.; Ma, J.; Shi, C.; Wu, W.; Wu, B. Enhanced temperature stability in high piezoelectric performance of (K, Na)NbO<sub>3</sub>-based lead-free ceramics through co-doped antimony and tantalum. *J. Alloy Compd.* **2021**, *852*, 156865. [[CrossRef](#)]
14. Liu, Y.-X.; Thong, H.-C.; Cheng, Y.-Y.-S.; Li, J.-W.; Wang, K. Defect-mediated domain-wall motion and enhanced electric-field-induced strain in hot-pressed K<sub>0.5</sub>Na<sub>0.5</sub>NbO<sub>3</sub> lead-free piezoelectric ceramics. *J. Appl. Phys.* **2021**, *129*, 024102. [[CrossRef](#)]
15. Hreščak, J.; Bencan, A.; Rojác, T.; Malič, B. The influence of different niobium pentoxide precursors on the solid-state synthesis of potassium sodium niobate. *J. Eur. Ceram. Soc.* **2013**, *33*, 3065–3075. [[CrossRef](#)]
16. Xie, Y.; Xing, J.; Tan, Z.; Xie, L.; Cheng, Y.; Wu, X.; Han, R.; Chen, Q.; Zhu, J. High mechanical quality factor and piezoelectricity in potassium sodium niobate ceramics. *Ceram. Int.* **2022**, *48*, 6565–6573. [[CrossRef](#)]
17. Kim, B.-H.; Yang, S.-A.; Lee, M.-K.; Lee, G.-J. Properties of (Bi,M)ZrO<sub>3</sub> (M: Alkali metals)-modified (K,Na)NbO<sub>3</sub> lead-free piezoceramics. *Ceram. Int.* **2017**, *43*, 15880–15885. [[CrossRef](#)]
18. Batra, K.; Sinha, N.; Kumar, B. Effect of Nd-doping on 0.95(K<sub>0.6</sub>Na<sub>0.4</sub>)NbO<sub>3</sub>-0.05(Bi<sub>0.5</sub>Na<sub>0.5</sub>)ZrO<sub>3</sub> ceramics: Enhanced electrical properties and piezoelectric energy harvesting capability. *J. Phys. Chem. Solids* **2022**, *170*, 110953. [[CrossRef](#)]
19. Wang, D.; Hussain, F.; Khesro, A.; Feteira, A.; Tian, Y.; Zhao, Q.; Reaney, I.M. Composition and temperature dependence of structure and piezoelectricity in (1-x)(K<sub>1-y</sub>Na<sub>y</sub>)NbO<sub>3</sub>-x(Bi<sub>1/2</sub>Na<sub>1/2</sub>)ZrO<sub>3</sub> lead-free ceramics. *J. Am. Ceram. Soc.* **2017**, *100*, 627–637. [[CrossRef](#)]
20. Tang, X.; Chen, T.; Liu, Y.; Zhang, J.; Zhang, T.; Wang, G.; Zhou, J. Composition dependence of phase structure and electrical properties in (0.98-x)K<sub>0.35</sub>Na<sub>0.65</sub>NbO<sub>3</sub>-0.02BaZrO<sub>3</sub>-xBi<sub>0.5</sub>Na<sub>0.5</sub>ZrO<sub>3</sub> ternary ceramics. *J. Alloy Compd.* **2016**, *672*, 277–281. [[CrossRef](#)]
21. Batra, K.; Sinha, N.; Kumar, B. Lead-free 0.95(K<sub>0.6</sub>Na<sub>0.4</sub>)NbO<sub>3</sub>-0.05(Bi<sub>0.5</sub>Na<sub>0.5</sub>)ZrO<sub>3</sub> ceramic for high temperature dielectric, ferroelectric and piezoelectric applications. *J. Alloy Compd.* **2020**, *818*, 152874. [[CrossRef](#)]
22. Bongkarn, T.; Chootin, S.; Pinitsoontorn, S.; Maensiri, S. Excellent piezoelectric and ferroelectric properties of KNLNTS ceramics with Fe<sub>2</sub>O<sub>3</sub> doping synthesized by the solid state combustion technique. *J. Alloy Compd.* **2016**, *682*, 14–21. [[CrossRef](#)]
23. Guo, J.; Xu, F.; Shang, X.; Lu, Y.; Li, P.; Zhou, T.; Zhang, Z.; He, Y.; Damjanovic, D. High-Performance Small-Amount Fe<sub>2</sub>O<sub>3</sub>-Doped (K,Na)NbO<sub>3</sub>-Based Lead-Free Piezoceramics with Irregular Phase Evolution. *J. Am. Ceram. Soc.* **2016**, *99*, 2341–2346. [[CrossRef](#)]
24. Cheng, Y.; Xing, J.; Li, X.; Xie, L.; Xie, Y.; Tan, Z.; Zhu, J. Meticulously tailoring phase boundary in KNN-based ceramics to enhance piezoelectricity and temperature stability. *J. Am. Ceram. Soc.* **2022**, *105*, 5213–5221. [[CrossRef](#)]
25. Yashima, M.; Omoto, K.; Chen, J.; Kato, H.; Xing, X. Evidence for (Bi,Pb)-O Covalency in the High TC Ferroelectric PbTiO<sub>3</sub>-BiFeO<sub>3</sub> with Large Tetragonality. *Chem. Mat.* **2011**, *23*, 3135–3137. [[CrossRef](#)]
26. Eichel, R.-A. Structural and dynamic properties of oxygen vacancies in perovskite oxides-analysis of defect chemistry by modern multi-frequency and pulsed EPR techniques. *Phys. Chem. Chem. Phys.* **2011**, *13*, 368–384. [[CrossRef](#)]
27. Malic, B.; Jenko, D.; Holc, J.; Hrovat, M.; Kosec, M. Synthesis of Sodium Potassium Niobate: A Diffusion Couples Study. *J. Am. Ceram. Soc.* **2008**, *91*, 1916–1922. [[CrossRef](#)]
28. Zhang, N.; Zheng, T.; Li, N.; Zhao, C.; Yin, J.; Zhang, Y.; Wu, H.; Pennycook, S.J.; Wu, J. Symmetry of the Underlying Lattice in (K,Na)NbO<sub>3</sub>-Based Relaxor Ferroelectrics with Large Electromechanical Response. *ACS Appl. Mater. Interfaces* **2021**, *13*, 7461–7469. [[CrossRef](#)]

29. Fu, J.; Zuo, R.; Xu, Z. High piezoelectric activity in (Na,K)NbO<sub>3</sub> based lead-free piezoelectric ceramics: Contribution of nanodomains. *Appl. Phys. Lett.* **2011**, *99*, 062901. [[CrossRef](#)]
30. Lin, D.; Zhang, S.; Cai, C.; Liu, W. Domain size engineering in 0.5%MnO<sub>2</sub>-(K<sub>0.5</sub>Na<sub>0.5</sub>)NbO<sub>3</sub> lead free piezoelectric crystals. *J. Appl. Phys.* **2015**, *117*, 074103. [[CrossRef](#)]
31. Zuo, R.; Fu, J.; Wang, X.; Li, L. Phase transition and domain variation contributions to piezoelectric properties of alkaline niobate based lead-free systems. *J. Mater. Sci. Mater. Electron.* **2009**, *21*, 519–522. [[CrossRef](#)]
32. Zheng, T.; Wu, J. Electric field compensation effect driven strain temperature stability enhancement in potassium sodium niobate ceramics. *Acta Mater.* **2020**, *182*, 1–9. [[CrossRef](#)]
33. Tao, H.; Yin, J.; Wu, W.; Zhao, L.; Ma, J.; Wu, B. Sharpening polycrystalline phase boundary for potassium sodium niobate ceramics with MnF<sub>2</sub> modification. *J. Am. Ceram. Soc.* **2022**, *105*, 5003–5010.
34. Tan, Z.; Peng, Y.; An, J.; Zhang, Q.; Zhu, J. Critical Role of Order-Disorder Behavior in Perovskite Ferroelectric KNbO<sub>3</sub>. *Inorg. Chem.* **2021**, *60*, 7961–7973. [[CrossRef](#)]
35. Jin, L.; Li, F.; Zhang, S.; Green, D.J. Decoding the Fingerprint of Ferroelectric Loops: Comprehension of the Material Properties and Structures. *J. Am. Ceram. Soc.* **2014**, *97*, 1–27. [[CrossRef](#)]
36. Cen, Z.; Bian, S.; Xu, Z.; Wang, K.; Guo, L.; Li, L.; Wang, X. Simultaneously improving piezoelectric properties and temperature stability of Na<sub>0.5</sub>K<sub>0.5</sub>NbO<sub>3</sub> (KNN)-based ceramics sintered in reducing atmosphere. *J. Adv. Ceram.* **2021**, *10*, 820–831. [[CrossRef](#)]